Journal of Sound and Vibration 329 (2010) 3958–3971

Contents lists available at ScienceDirect

Journal of Sound and Vibration

journal homepage: www.elsevier.com/locate/jsvi

Measuring surface pressure with far field acoustics

William Devenport [a,*], Elisabeth A. Wahl [a], Stewart A.L. Glegg [b], W. Nathan Alexander [a], Dustin L. Grissom [a,1]

[a] Virginia Tech, Aerospace and Ocean Engineering Department, 215 Randolph Hall, Blacksburg, VA 24061, USA
[b] Florida Atlantic University, Ocean Engineering Department, Boca Raton, FL 33431, USA

ARTICLE INFO

Article history:
Received 8 June 2009
Received in revised form
6 February 2010
Accepted 10 March 2010
Handling Editor: P. Joseph
Available online 11 May 2010

ABSTRACT

This paper presents measurements of the wavenumber frequency spectrum of wall pressure fluctuations under a turbulent boundary layer made using sound radiated from hydrodynamically smooth ridges in the surface. The measurements also serve as a test of the scattering theory of roughness noise. The radiated sound reveals a cut through the full three-dimensional wavenumber frequency spectrum of the wall pressure at the wavenumber of the surface. Since ridges can be made with very small wavelengths, this technique can be used to probe the structure of the wall pressure spectrum on scales far smaller than those that can be reached using conventional wall-mounted transducers. Furthermore, the method reveals the wavenumber frequency spectrum directly, without the need for multi-point measurements or the spatial Fourier transforming of data. Measured spectra bear a close similarity to Corcos' and Chase's model forms, and confirm the applicability of the theory of roughness noise and its prediction of roughness noise directivity.

1. Introduction

This paper addresses both the direct measurement of the wavenumber frequency spectrum of wall pressure fluctuations in a turbulent boundary layer and the validation of the scattering theory of roughness noise. The spectrum, which separates the pressure fluctuations by both streamwise and spanwise wavenumber, as well as frequency, is an important descriptor of the turbulent boundary layer structure. From an engineering point of view it provides the source term needed for calculations such as the structural response of a panel or window over which the boundary layer is growing (e.g. [1]) or the roughness noise radiated by the surface [2]. From the scientific perspective it provides a detailed statistical view of the turbulence structure of the boundary layer weighted in favor of the near-wall region where the flow physics is least understood. There are relatively few explicit measurements of the wavenumber-frequency spectrum, particularly in its three-dimensional form and at high wavenumbers (small scales). The reason is the need to rely on pressure transducers mounted at the wall itself. Whether the pressure transducers are used as point-wise measurement devices (e.g. [1,3]) or their finite size is employed as part of a wavenumber filter strategy (e.g. [4,5]), large numbers of transducers or measurements are needed to determine even small portions of the wavenumber frequency spectrum. This is particularly true if separation of streamwise and spanwise wavenumbers is desired. The finite size of transducers usually limits measurements to spatial scales of typically 10 mm or more, with sometimes unknown aliasing effects. This is not a small scale compared to most boundary layer thicknesses.

When a boundary layer flows over a rough surface, the fluctuating wall pressure field is scattered by the surface to produce sound of dipole order. Until recently, the experimental data on roughness noise was limited and there was little on which to

* Corresponding author. Tel.: +1 540 231 4456.
E-mail address: devenport@vt.edu (W. Devenport).
[1] Currently at: Raytheon Missile Systems, Tucson, AZ, USA.

0022-460X/$ - see front matter © 2010 Elsevier Ltd. All rights reserved.
doi:10.1016/j.jsv.2010.03.012

base the development or testing of theoretical models. In the last few years this subject has seen increased attention with new measurements by Grissom et al. [6], Smith et al. [7], Anderson et al. [8], and Liu et al. [9]. This has led to new theoretical developments, in particular a comprehensive theory for roughness noise [2]. The new theory, in which the roughness noise is seen to be the result of a convolution between the surface pressure wavenumber frequency spectrum, and the wavenumber spectrum of the rough surface slope, shows some consistency with experiments. In particular, it predicts the roughness noise for stochastic surfaces should scale on the wall pressure spectrum, the ratio between the two being proportional to the square of the frequency and the square of the roughness height—consistent with the measurements for sandpaper surfaces of Smith et al. [7]. The ability of theory to predict the roughness noise directivity has not been tested, however, nor has the validity of the theory been examined for the much more carefully controlled case of a deterministic surface. The purpose of this paper is to present the results of just such a test—a test that also demonstrates the direct measurement of the wall pressure wavenumber frequency spectrum of a turbulent boundary layer using farfield sound.

2. Theoretical basis

Following the analysis of Glegg and Devenport [2], consider a rough or textured surface in the y_1,y_3 plane with a surface elevation $y_2=\xi(y_1,y_3)$, subjected to a homogeneous fluctuating hydrodynamic pressure field, p_s. As can be established directly from Lighthill's equation, with an appropriate selection of the Green's function, the pressure fluctuations will scatter off the surface generating sound. The pressure field associated with the sound p heard at position $\mathbf{x}$ and frequency ω is

$$p(\mathbf{x},\omega)\approx\frac{2\pi ik_o e^{ik_o|\mathbf{x}|}}{|\mathbf{x}|}\int_\kappa p_s(k_1,k_3,\omega)\frac{\mathbf{x}.\boldsymbol{\zeta}(k_1,k_3)}{|\mathbf{x}|}\,\mathrm{d}k_1\,\mathrm{d}k_3 \tag{1}$$

Here k_1 and k_3 are the wavenumbers corresponding to y_1 and y_3, and k_o is the acoustic wavenumber. The surface pressure appears in terms of its Fourier transform with respect to y_1,y_3 and time p_s. The function $\boldsymbol{\zeta}$ is the vector wavenumber spectrum of the surface gradient, i.e.

$$\zeta^{(j)}(k_1,k_3)=\frac{1}{(2\pi)^2}\int_\Sigma\frac{\partial\xi}{\partial y_j}e^{\mathrm{i}(k_1y_1+\mathrm{i}k_3y_3)}\mathrm{d}\Sigma\quad j=1,3 \tag{2}$$

where Σ is the area of the surface projected on to the y_1,y_3 plane. This result, which has been simplified by assuming the variations in surface height are small compared to the acoustic wavelength, forms the basis of the theory of roughness noise. It shows that the sound spectrum is essentially the result of wavenumber filtering of the wall pressure. The filter is the wavenumber transform of the surface slope taken in the direction of the observer.

This filtering interpretation of the scattering equation suggests an application other than in the prediction of roughness noise. Specifically it implies that one can tailor the shape of a designed surface to reveal specific aspects of the wavenumber content of the wall pressure. In other words, one can design the surface like a diffraction grating, to separate out the particular spectral components desired. For such a scheme to be successful it is necessary that the resulting surface elevations be small enough so as not to disturb the flow passing over it.

Consider for example the sound radiated by flow over a wall with a periodic pattern of sinusoidal ribs with wavenumber vector $\mathbf{k_w}=(k_w^{(1)},k_w^{(3)})$. In this case

$$\xi=a\cos(k_w^{(1)}y_1+k_w^{(3)}y_3) \tag{3}$$

The spectrum of the surface gradient in this case, from Eq. (2), is given by

$$\begin{aligned}\zeta^{(1)}(k_1,k_3)&=\frac{ik_w^{(1)}a}{2}[\delta(k_1+k_w^{(1)})\delta(k_3+k_w^{(3)})-\delta(k_1-k_w^{(1)})\delta(k_3-k_w^{(3)})]\\ \zeta^{(3)}(k_1,k_3)&=\frac{ik_w^{(3)}a}{2}[\delta(k_1+k_w^{(1)})\delta(k_3+k_w^{(3)})-\delta(k_1-k_w^{(1)})\delta(k_3-k_w^{(3)})]\end{aligned} \tag{4}$$

and so from Eq. (1)

$$p(\mathbf{x},\omega)\approx\frac{-\pi k_o a e^{ik_o|\mathbf{x}|}}{|\mathbf{x}|^2}\mathbf{k}_w.\mathbf{x}[p_s(k_w^{(1)},k_w^{(3)},\omega)-p_s(-k_w^{(1)},-k_w^{(3)},\omega)] \tag{5}$$

By squaring this equation and taking the expected value one gets the expression for the power spectrum of the radiated sound $S_{pp}(\mathbf{x},\omega)=(\pi/T)Ex[|p|^2]$ as

$$S_{pp}(\mathbf{x},\omega)\approx\left(\frac{\pi k_o a}{|\mathbf{x}|^2}\mathbf{k}_w.\mathbf{x}\right)^2\left(\frac{\Sigma}{\pi^2}\right)[\Phi_{PP}(k_w^{(1)},k_w^{(3)},\omega)+\Phi_{PP}(-k_w^{(1)},-k_w^{(3)},\omega)] \tag{6}$$

where $\Phi_{pp}(k_1,k_3,\omega)$ is the wavenumber frequency spectrum of the surface pressure. The scattering process picks out the specific components of the wall pressure spectrum at the wavenumber that describes the surface. Thus by measuring the radiated sound one can measure the frequency dependence of the surface pressure wavenumber spectrum at the wavenumber $\mathbf{k_w}$.

By rotating a single sinusoidal surface to different angles, such sound measurements could be used to map out a complete cylindrical cut through the three dimensional wavenumber frequency space of the wall pressure spectrum at the wavenumber magnitude of the surface. In principle, by using a set of such surfaces of different wavelength, one could map

the entire space. Such a technique might be particularly useful for probing the wall pressure spectrum at small scales where conventional measurements with pairs of transducers are not possible.

3. Experimental setup

3.1. Wind tunnel

Experiments were made in the low-speed wall-jet wind tunnel described in detail by Grissom [10], Smith [11] and Smith et al. [7]. The facility (Fig. 1) is powered by a centrifugal blower that drives air through a silencer and an acoustically treated settling chamber to a 1206 mm-wide two-dimensional nozzle of adjustable height. The jet emerging from the nozzle flows over a wide and long flat plate forming a wall jet consisting of a boundary layer flow adjacent to the flat plate topped by a mixing layer. The wall-jet configuration allows far field noise radiated from a surface to be measured without the need to place microphones in or near the flow. The fairly rapid streamwise decay of the wall jet ensures that any edges (and potential scattering sources) can be positioned away from regions of significant flow velocity.

Detailed discussion of the aerodynamic properties of the wall jet is provided by Grissom et al. [6] and Smith et al. [7] which were measured using Pitot static and hot-wire anemometry. As far as 1.85 m downstream of the nozzle exit, the wall jet is still two dimensional over an 800 mm wide core. Mean velocity profiles measured on the centerline of the jet show a wall-jet boundary layer closely consistent with the expectations of self-similarity, as detailed by Narasimha et al. [12] and Wygnanski et al. [13]. As such the boundary layer displacement thickness δ^* and wall-jet maximum velocity U_m can be accurately described as functions of the nozzle exit velocity U_j, nozzle height b and streamwise position from the nozzle x as

$$\frac{U_m}{U_j} = 4.97\,\mathrm{Re}_j^{n+1}\mathrm{Re}_x^n \tag{7}$$

$$\frac{\delta_*}{b} = 0.0156\,\mathrm{Re}_j^{m-2}\mathrm{Re}_x^m \tag{8}$$

Here $Re_j = U_j b/\nu$ and $Re_x = U_j x/\nu$. The empirical exponents n and m are -0.512 and 0.888, respectively. The self-similarity of the boundary layer profile means that the different measures of the thickness are in almost constant proportion with the overall boundary layer thickness $\delta \approx 15.4\delta^*$ and the momentum thickness $\theta \approx 0.74\delta^*$. Note that wall jet boundary layer profiles are fuller than typical external flow boundary layers and hence the large value of δ/δ^*. The relations for the boundary layer thicknesses differ from those presented by Smith et al. [7] since they include the effect of the acoustically treated enclosure placed over the wall jet during acoustic measurements.

3.2. Ribbed surface

The two-dimensional roughness used for these tests is a patch of lenticular lens material. This material, used for creating the appearance of moving or three-dimensional images, has tight tolerances on surface shape and finish. The lens is produced by Micro Lens Technology Inc. and is designated as Flip LPI 20. The surface used here had a ridge spacing of 1.26 mm (see Fig. 2) and height of 0.31 mm. In profile the ridges are not sinusoidal but form a succession of elliptical arcs.

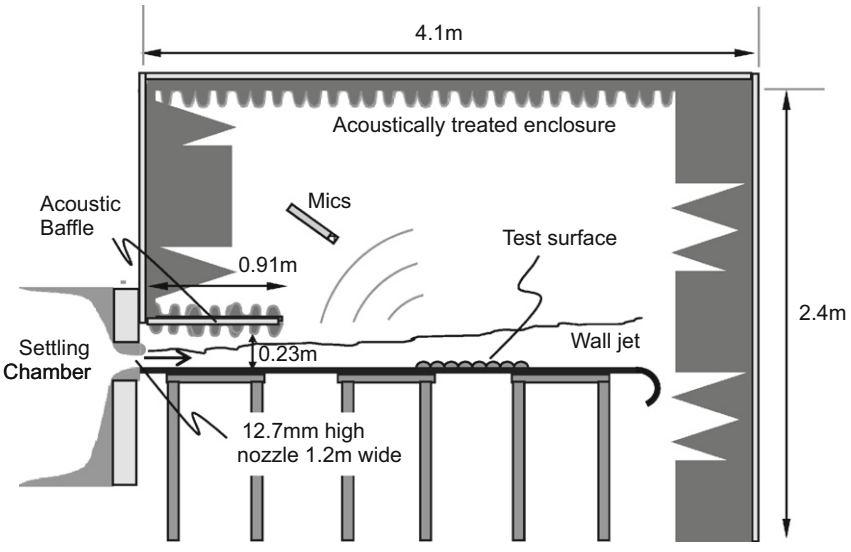

Fig. 1. Side-view schematic of the Virginia Tech Roughness Noise Wind Tunnel.

However, a Fourier decomposition shows that the fundamental sinusoidal component of the shape has a mean square amplitude some 10 times greater than the first harmonic, and the contribution from higher harmonics decays rapidly from there. Contributions to the radiated sound spectrum, as per Eq. (6), from the harmonics would therefore be expected to be small. The amplitude of the fundamental sinusoidal component of the surface, a, is 0.10 mm.

The LPI 20 surface was selected as the most suitable from a limited set of available lens sizes. Ideally, one wants the surface amplitude to be large enough to generate sound at a level that can be easily measured (Eq. (6)) and small enough to have no effect on the turbulent boundary layer growing over it. These conflicting requirements suggest that the ideal surface would have an amplitude of the order of the sublayer thickness.

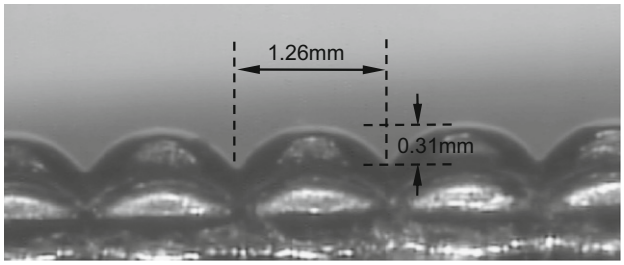

Fig. 2. Microscope image showing the profile of the lenticular lens sheet.

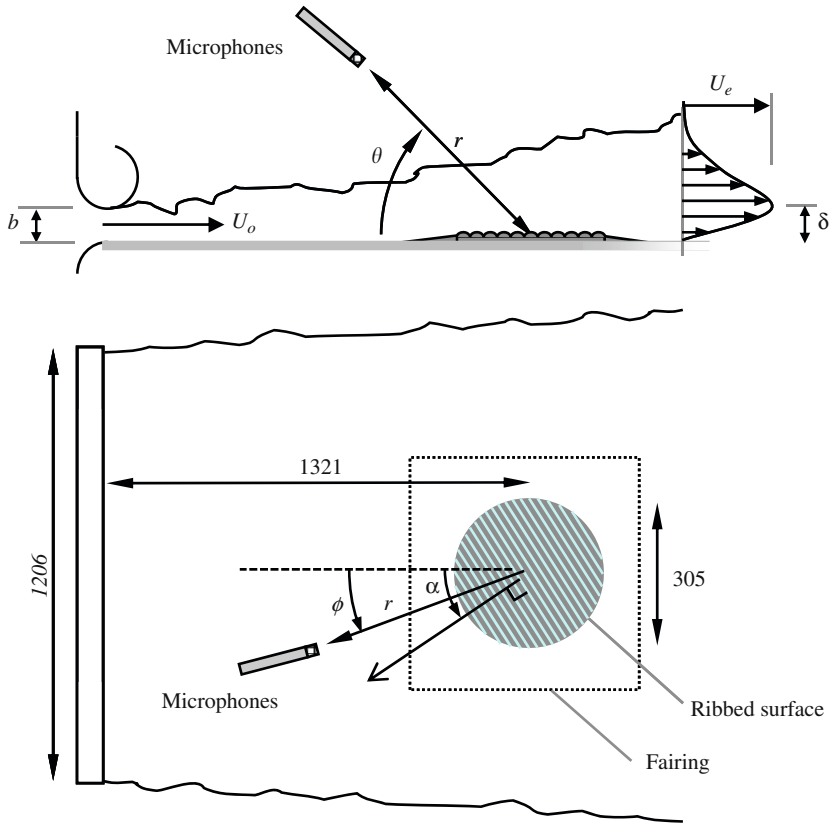

mic no.	r	θ	ϕ
1	542	56.6	-1.2
2	538	55.2	20.1
3	581	54.6	40.5
4	837	53.3	62.6

Fig. 3. Schematic showing the measurement setup.

A circular fetch 305 mm in diameter, was used. The overall thickness of the lens sheet is 2.1 mm so to avoid a step at the edge of the lens sheet the fetch was embedded in a close-fitting circular hole in the center of a 3.2 mm thick square aluminum plate 457 mm on edge, see Fig. 3. The outer 38 mm margin of the plate was faired down to form a ramp to provide a smooth and quiet transition from the surrounding surface. The outer edge of the ramp was covered with 0.06 mm thick cellophane tape to prevent any gaps. The embedded lens sheet was shimmed up to eliminate any discernable step between it and the surrounding plate (<0.06 mm measured to the tops of the ribs).

3.3. Flow properties over the ribbed surface

The fetch was placed with its center a distance of 1321 mm downstream of the nozzle exit, see Fig. 3. Acoustic measurements were made for a nozzle height b of 12.7 mm and nozzle exit velocities U_j of 40 and 60 $\mathrm{m\,s^{-1}}$. At these conditions the boundary layer thicknesses (δ, δ^* and θ) at the center of the fetch, computed using Eq. (8) and the accompanying ratios, would have been 19, 1.2 and 0.9 mm for 40 $\mathrm{m\,s^{-1}}$ and 17, 1.1 and 0.8 mm for 60 $\mathrm{m\,s^{-1}}$. Eq. (7) gives edge velocities close to 36 percent of the nozzle exit velocity for both speeds. These numbers combine to give boundary layer momentum thickness Reynolds numbers of 760 and 1040 at the two speeds. Using the skin friction correlation of Bradshaw and Gee [14] for fully developed wall jets, $C_f=0.0315(U_m\delta/\nu)^{-0.182}$, the viscous lengthscale ν/U_τ is estimated as 0.016 mm at 60 $\mathrm{m\,s^{-1}}$ and 0.023 mm at 40 $\mathrm{m\,s^{-1}}$. Thus the amplitude of the ribs would have corresponded to about 6 wall units and 4 wall units, respectively. Growth and decay of the wall-jet boundary layer over the fetch would have resulted in a ± 10 percent variation in boundary layer thickness, ± 5 percent variation in edge velocity, and no significant variation in viscous lengthscale.

These values, of course, assume that the boundary layer was not significantly affected as it flowed over the ribbed surface and the surrounding aluminum ramp. This assumption was checked by using hot-wire anemometry to measure profiles close to the downstream edge of the fetch (at $x=1470$ mm) with the ribs oriented spanwise and streamwise. The measurements were made for a jet velocity of 60 $\mathrm{m\,s^{-1}}$ and immediately preceded and followed by profiles measured at the same location, but with the fetch and the surrounding ramp removed. Mean velocity and turbulence intensity profiles are shown in Fig. 4. Note that the y locations of the profiles had to be shifted slightly (<0.5 mm) to correct for uncertainty in the initial positions of the hot-wire sensor for each profile. Normalized on U_m and δ these show no visible effect of the ribbed surface. In absolute form, however, both profiles measured with the ribs both showed a slightly higher maximum velocity U_m, the difference being close to 1 percent of U_j. We believe this to be an effect of the small curvature of the wall jet produced by the displacement of the flow over the aluminum ramp surrounding the fetch, and not a direct effect of the ribs.

3.4. Instrumentation

Four B&K model 4190 free-field 1/2-in microphones were used. These have a high sensitivity, low noise contamination, and flat frequency response to over 20 kHz. These microphones were used in conjunction with a B&K Nexus 2690 A0S4

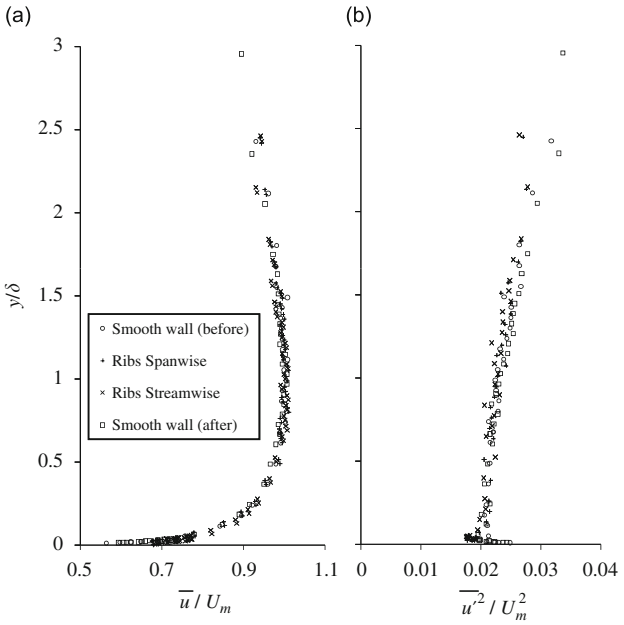

Fig. 4. Profiles of (a) mean velocity and (b) streamwise turbulence normal stress measured at $x=1470$ mm with and without the ribbed surface and surrounding ramp, for a jet exit velocity of 60 m/s.

amplifier and were calibrated using a B&K model 4228 pistonphone. Microphone outputs were measured using an Agilent E1432 16-bit digitizer. Spectra presented here are the result of averaging 1000 records of 2048 samples recorded at 51 200 Hz for each condition. Before digitizing, the microphone signals were high pass filtered at 250 Hz to reduce low frequency contamination.

The four microphones were placed between 538 and 837 mm from the center of the fetch at vertical receiver angles θ of close to 55° and horizontal receiver angles ϕ varying from $-1.2°$ to 62.6°, see Fig. 3 and the embedded table. The microphones positions were chosen to give the widest range or receiver angles possible while remaining within the region where most of the background noise emanating from the nozzle area was blocked by the acoustic baffle (see Fig. 1). All the microphone positions lie near a spanwise line 440 mm above the flow surface and 300 mm upstream of the center of the fetch.

4. Results

4.1. Signal to noise ratio

The wall pressure measurement scheme that has been outlined depends on the scattering of sound from a sinusoidal surface where the ribs are so small as to be hydrodynamically smooth, or nearly so. It is reasonable therefore to question whether such sounds could be heard above noise generated by the rest of the flow, the edges of the fetch, or the facility background. This question is answered in Fig. 5, which compares sound measurements made with the circular fetch at various angles α (see Fig. 3) with those made with the fetch removed, leaving an entirely smooth surface. Measurements were made using microphone 1 placed upstream of the center of the fetch ($\phi=-1.2°$) for nozzle exit velocities of 40 and 60 ms^{-1}.

When the plate is entirely smooth, the background sound levels come from the noise of the jet and/or nozzle and follow a roughly straight line in the log–log scale with a slope of about -3. There appear to be no earlier measurements of two-dimensional wall jet noise for similar conditions, but this slope is at least approximately consistent with the high frequency roll off in noise from a rectangular subsonic jet as seen by an observer at almost the same angle to the jet axis (see [15]). The sound for the clean plate is louder at lower frequencies and quieter at higher frequencies. Overall, smooth plate sound levels are about 15 dB lower for 40 ms^{-1} than 60 ms^{-1}. At 60 ms^{-1}, with the fetch installed and oriented at $\alpha=0°$ (ridges perpendicular to the flow), the sound spectra show an increase that begins around 5 kHz and reaches a broad peak with a maximum around 10 kHz. This sound generated by the fetch is clearly audible over the background levels with a signal to noise ratio of about 13 dB. For 40 ms^{-1}, the peak occurs at a lower frequency, 8 kHz, and the peak signal to noise ratio is about 7 dB. When the patch is oriented at $\alpha=90°$ and the ribs are parallel to the flow, the theory of Eq. (6) indicates that there will be no sound from the ribbed surface. Indeed, the figure shows no discernable sound above the background at either speed when the ridges are at 90°. This also demonstrates that no significant sound is generated by the edges of the disc or the surrounding aluminum fairing. When the ribs are positioned at $\alpha=41°$ the signal to noise ratio drops by approximately half to 8 dB at 60 ms^{-1} and 4 dB at 40 ms^{-1}. At 60°, the signal to noise ratio is only 1 dB for the 60 ms^{-1} case and no signal can be distinguished at 40 ms^{-1}.

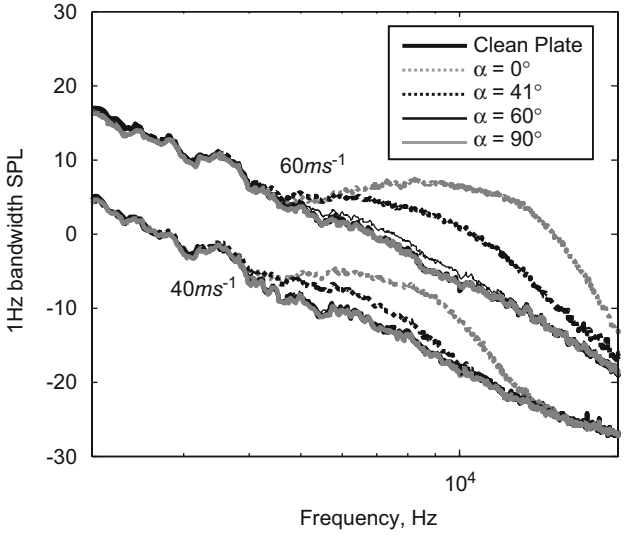

Fig. 5. Measurements of the sound spectrum (in terms of 1 Hz bandwidth SPL) in the presence of the circular fetch of lenticular lens sheet at various angles and speeds, as compared to that radiated with the fetch and surrounding plate removed so as to produce an entirely smooth surface.

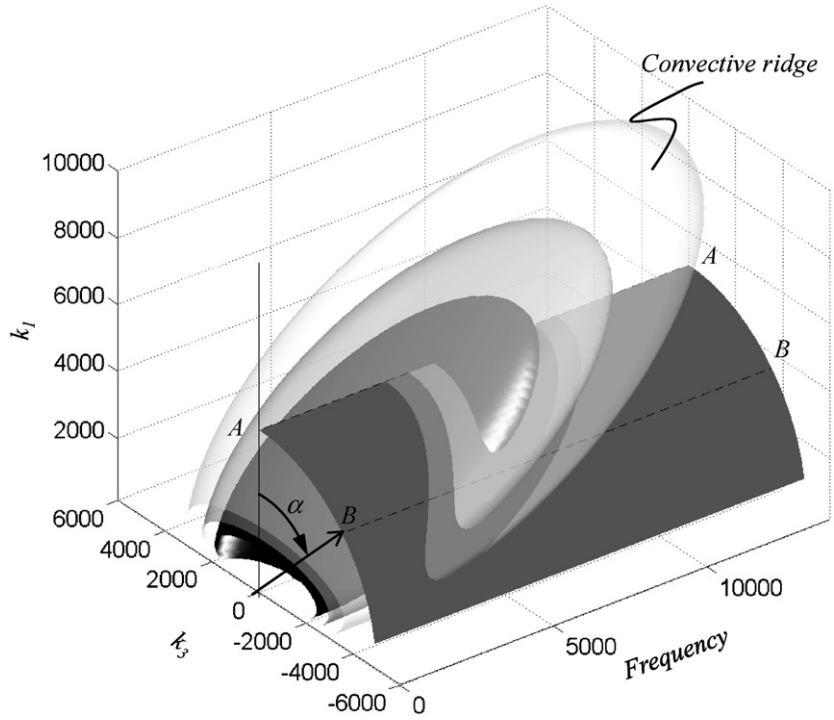

Fig. 6. Schematic showing isosurfaces of the wall pressure wavenumber frequency spectrum (plotted using [18] model) and the location of the measured cuts AA and BB.

The peaked form of the sound spectra produced by the ribs can be explained with reference to the wavenumber frequency spectrum of the wall pressure. Fig. 6 shows the form of this spectrum which is dominated by the convective ridge centered on an inclined plane that lies perpendicular to the k_1, ω plane. The slope of the convective ridge in the k_1, ω plane is determined by the convection velocity of the boundary layer pressure fluctuations. Following Eq. (6), the additional sound scattered by the ribbed surface for $\alpha=0^\circ$ should represent a cut AA through the convective ridge at the wavenumber for $k_1=k_w$ and $k_3=0$. As the patch is rotated, the wavenumber vector takes on components in k_1 and k_3 and will create a different slice through the convective ridge, e.g. BB. Furthermore, the peak value of the sound should move toward lower frequencies because of the slope of the convective ridge, much as is seen in the present data in Fig. 5. The loudest sound should be heard in the frequency band of the convective ridge.

Before these sound spectra, and others like them can be used to quantitatively determine the form of the wall pressure spectrum it is necessary to, as far as possible, remove the contribution from the background jet noise. This contribution not only increases the apparent levels but, since it falls off with frequency, can shift the apparent frequency of the convective ridge. Since the jet noise and noise from the ribs should be uncorrelated, decontamination is a simple matter of subtracting the sound spectra measured with the smooth wall from those measured with the ribs at the same flow speed. To reduce the uncertainty in the subtraction process at low signal to noise ratios (SNRs) the narrow band spectral levels were first combined into 1/10th octave bands. Even then, the subtraction was only performed if the SNR was greater than 1 dB. If not, the data were discarded. Spectra of the sound radiated by the ribs determined in this way, are presented and discussed in the following sections.

4.2. Detailed sound measurements

Far field sound measurements were made at 40 and 60 ms^{-1} with all four microphones (representing 4 distinct receiver angles) at 11 fetch orientations from 0° to 60°. The ultimate objective of these measurements was to sweep out a detailed cylindrical cut through the wall pressure wavenumber spectrum, as shown in Fig. 6. However, the discussion begins by using these results to show the directivity of the sound produced by the fetch, and the dependence of the sound on the angle of the ribs.

4.2.1. Directivity

Fig. 7(a) shows sound spectra recorded at 40 and 60 ms^{-1} with the ribs perpendicular to the flow direction ($\alpha=0^\circ$) as a function of the horizontal receiver angle ϕ. At both speeds the highest sound levels are recorded immediately in front of the patch at $\phi=-1.2^\circ$. As discussed above, these peaked spectra represent a cut at the wavenumber of the surface through

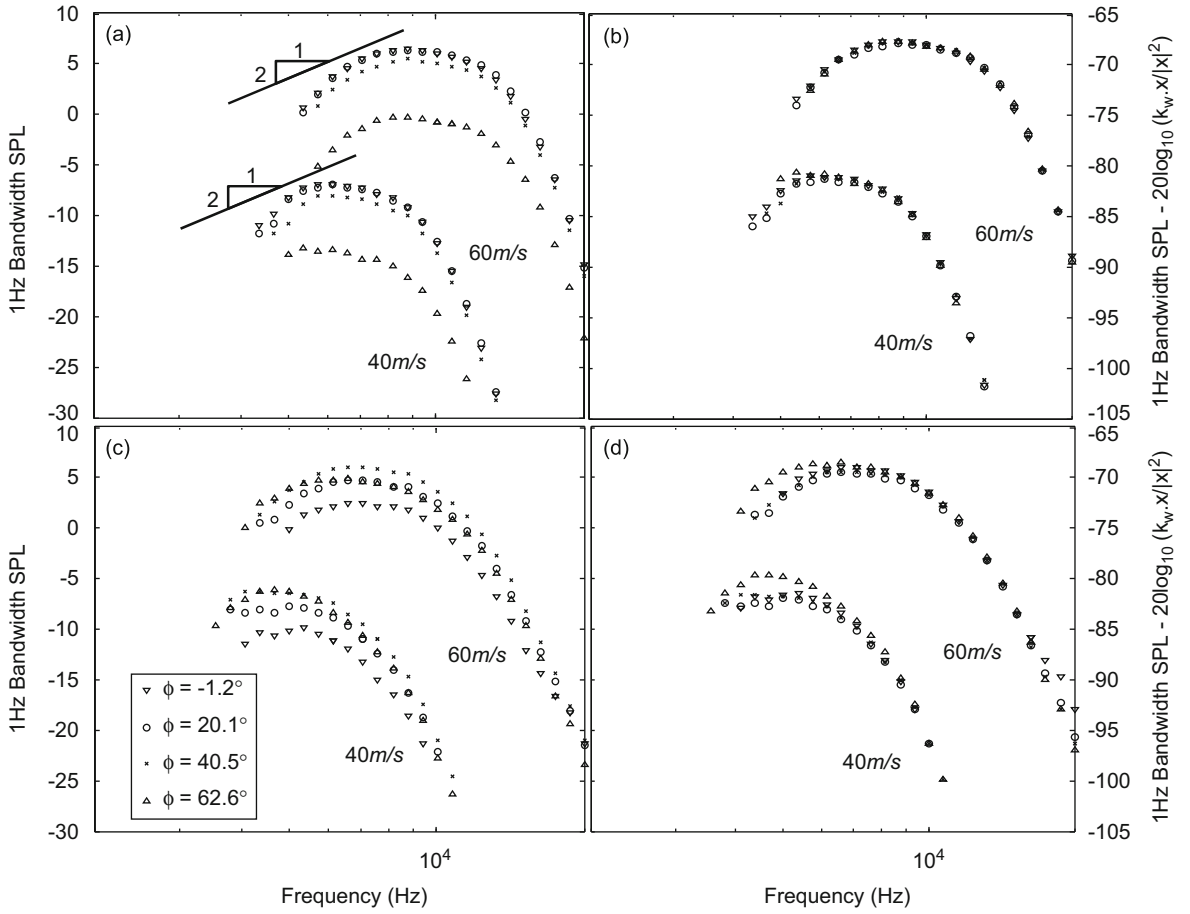

Fig. 7. Sound spectra recorded from different receiver angles (ϕ) with the circular lens sheet at angles of (a) 0° and (c) 41°. Parts (b) and (d) show the same data as (a) and (c) but with sound levels normalized on $(\mathbf{k_w \cdot x}/|\mathbf{x}|^2)^2$.

the convective ridge of the wall pressure spectrum. Since the sound spectrum is weighted by frequency squared compared to the wall pressure wavenumber spectrum (see Eq. (6)) one can, by comparing with a line of slope 2, infer that the latter peaks at a frequency of about 5 kHz at 40 ms^{-1} or 7 kHz at 60 ms^{-1}. This peak will correspond to the center of the convective ridge. Converting these to angular frequency and dividing by the wavenumber of the surface k_w=5000 rad m^{-1}, results in phase speeds of 6.3 and 8.8 ms^{-1}, respectively, about 44 and 41 percent of the average boundary layer edge velocity over the fetch for the 40 and 60 ms^{-1} cases. These numbers are a little lower than the notional phase speeds inferred from a two-point streamwise pressure cross spectrum in conventional boundary layers of about 60 percent (e.g. [16]). In a wall jet boundary layer convection speeds may be reduced by the impact of slower moving turbulence in the over-riding mixing layer. However, it is also worth noting that rather than its integral in wavenumber, a cut through the complete three-dimensional wavenumber frequency spectrum is being examined. This spectrum is being viewed on a wavenumber scale much smaller than that which is normally visible. To make the present measurement with surface pressure transducers, one would require a two-dimensional array of transducers with a spacing of no more than 0.63 mm.

Fig. 7(a) shows that sound levels drop as the horizontal receiver angle ϕ is increased from 0°. The drop is about 1 dB for ϕ=40.5° (microphone 3) and 7 dB for ϕ=62.6° (microphone 4). According to Eq. (6), varying the observer position $\mathbf{x}$ varies only the directivity/spherical spreading term $\mathbf{k_w \cdot x}/|\mathbf{x}|^2$, hence the magnitude of the spectrum should change but not the shape. Normalizing levels by this term (Fig. 7(b)) closely collapses the spectra measured at each speed by the different microphones confirming this expectation and demonstrating that Eq. (6) accurately captures the directivity of the measured sound.

Figs. 7(c) and 6(d) shows similar plots, but for a fetch angle of α=41°. Rotating the fetch changes the relative magnitudes of the spectra measured by the different microphones as well as their form (compare Figs. 7(c) and (a)). Indeed, the loudest sound is now recorded by microphone 3 at ϕ=40.5°. Normalizing on $\mathbf{k_w \cdot x}/|\mathbf{x}|^2$ again, see Fig. 7(d), still produces a good collapse of the data, the sole exception being the lowest frequency parts of the spectrum at a receiver angle of 62.6°. The reason for this discrepancy is not immediately clear, but we note that this particular measurement had the lowest signal to noise ratio of any of those represented in Fig. 7.

At first sight, the collapsed form of the spectra at 40 and 60 m s^{-1} appears quite similar (Figs. 7(b) and 6(d)) and it is tempting to infer that a simple velocity scaling exists. This is not the case, however. On careful inspection the spectra at 40 and 60 m s^{-1} have different shapes; the peak being broader and more hump-backed at 60 m s^{-1}. Normalizing the frequency on velocity does align the peaks quite well (particularly the high frequency roll-off) but the difference in peak levels (12–13 dB) is more than would be expected if the boundary layer scaling were simply accomplished by multiplying all velocities by 1.5 (9 dB). The true boundary layer scaling is, of course, more complicated and it is likely that in this case viscous effects play a substantial role in the changes seen on this very small physical scale and at these relatively low momentum thickness Reynolds numbers.

4.2.2. Effects of surface orientation α

Figs. 8 and 9 show sound spectra measured at the four microphone locations as a detailed function of the fetch angle α for 60 and 40 m s^{-1}, respectively. In all cases the noise from the ribs can be heard at frequencies above 3 kHz. As in Fig. 7, the spectra at 40m s^{-1} appear qualitatively identical to those measured at 60 m s^{-1} at least over the frequency ranges where the signal can be heard above the background. However, as before a simple quantitative scaling on speed does not work as there are differences in the shapes of the peaks and the increase in sound level with speed is greater than that which would be predicted from a simple inviscid scaling.

The results show strong effects of surface orientation. Rotating the fetch changes the direction of the wavenumber vector $\mathbf{k_w}$, not only affecting the value of dot product $\mathbf{k_w \cdot x}$ appearing in Eq. (6), but also the cut through the wavenumber spectrum that is revealed in the scattered sound. As a result, the sound spectra not only reduce in magnitude as the fetch is rotated, they change shape, with the peak sound level occurring at a lower frequency. This can be explained with reference to the schematic in Fig. 6. The measurements appear to conform well to these expectations. Consider the 60 m s^{-1} case, for a receiver angle of $\phi = -1.2^\circ$ (Fig. 8(a)). At $\alpha = 0^\circ$, the most intense sound is heard at approximately 9 kHz and is measured as 6 dB, but by $\alpha = 41^\circ$ the peak frequency has dropped to about 7 kHz and the level to 2 dB. The larger the angle, the quieter the sound is and the lower the frequency where the peak occurs. At $\alpha = 60^\circ$, the peak is no longer resolved and only a small amount of sound can be distinguished over the background. Similar behavior is seen in Fig. 8(a), showing the 40 m s^{-1} case for a receiver angle of -1.2°. Here the peak for $\alpha = 0^\circ$ occurs at approximately -7 dB. This is 13 dB quieter than the 60 m s^{-1} case. The peak also moved from 10 to 7 kHz. No discernable sound can be heard for angles above $\alpha = 53^\circ$ at this speed.

The remaining parts of Figs. 8 and 9 show the effects of fetch orientation seen at the other receiver angles. Ignoring the fact that changing the fetch orientation changes the part of Φ_{PP} that is radiated, one would expect sound levels to be controlled by the dot product $\mathbf{k_w \cdot x}$ appearing in Eq. (6), and thus largest when the receiver angle and fetch angle match.

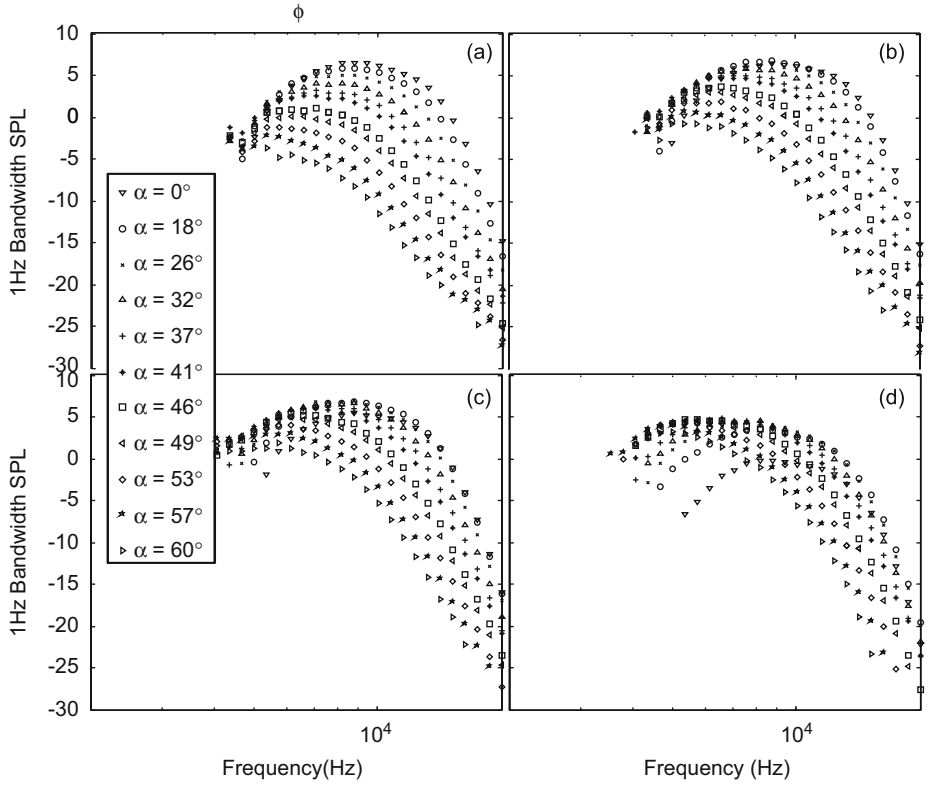

Fig. 8. Sound spectra recorded for different surface rib angles (α) at 60 m s^{-1} at receiver angles of (a) $\phi = -1.2^\circ$, (b) $\phi = 20.1^\circ$, (c) $\phi = 40.5^\circ$ and (d) $\phi = 62.6^\circ$.

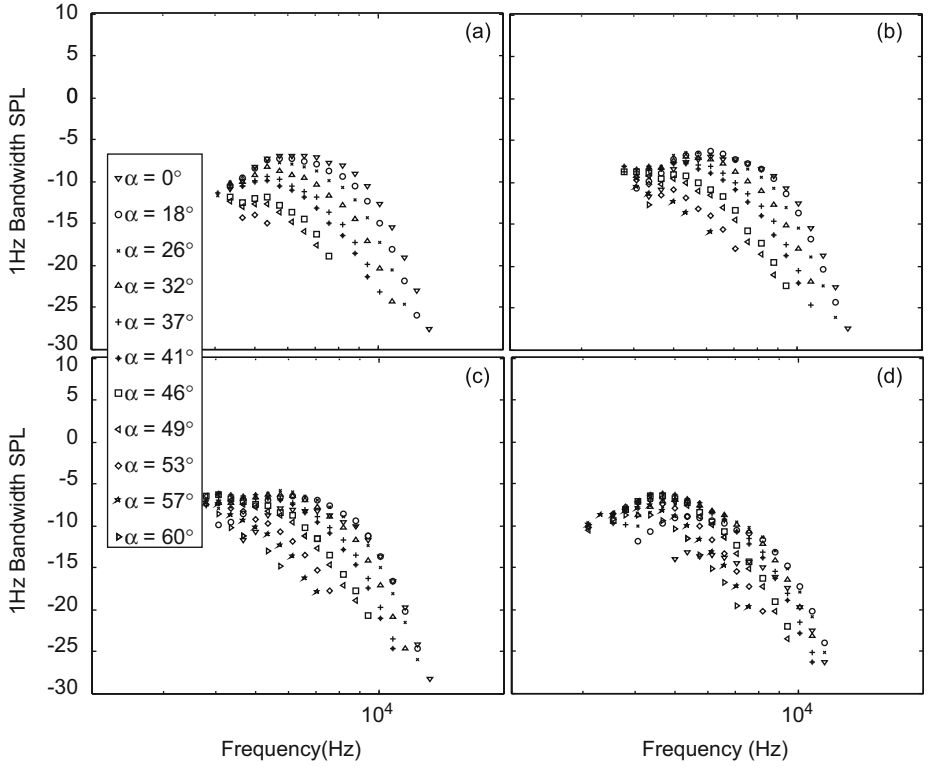

Fig. 9. Sound spectra recorded for different surface rib angles (α) at 40 ms^{-1} at receiver angles of (a) $\phi=-1.2^\circ$, (b) $\phi=20.1^\circ$, (c) $\phi=40.5^\circ$ and (d) $\phi=62.6^\circ$.

This is true for microphone 1 ($\phi=-1.2^\circ$, Figs. 8(a) and 9(a)), microphone 2 at lower frequencies ($\phi=20.1^\circ$, Figs. 8(b) and 9(b)), but does not occur at the other two microphone locations (Figs. 8(c),(d) and 9(c),(d)) because of the decrease in the peak frequency of the sound spectra as the fetch is rotated. These variations are best explained and correlated by using the data to directly estimate the shape and form of the wavenumber frequency spectrum of the wall pressure, using Eq. (6).

4.3. The form of the wavenumber spectrum of wall pressure

The measured sound spectra can be used to explicitly estimate the wavenumber frequency spectrum of the wall pressure fluctuations, at the wavenumber of the ribbed surface, through an elementary rearrangement of Eq. (6).

$$\mathbf{\Phi}_{PP}(k_w^{(1)},k_w^{(3)},\omega)=\frac{S_{pp}(\mathbf{x},\omega)}{\left(\dfrac{\pi k_o a}{|\mathbf{x}|^2}\mathbf{k_w}.\mathbf{x}\right)^2\left(\dfrac{\Sigma}{\pi^2}\right)} \tag{9}$$

Note that this implicitly assumes that the negative wavenumber component of Φ_{PP} is negligible. Specifically, for a given speed, each set of spectra measured by a single microphone provides a two-dimensional estimate (with frequency and wavenumber angle $\alpha=\arctan(k_3/k_1)$) of the wall-pressure wavenumber frequency spectrum over the cylindrical cut shown schematically in Fig. 6. Furthermore, the estimates obtained from the different microphones should be the same.

Absolute wavenumber frequency spectra inferred from the four sets of microphone measurements at 60 ms^{-1} are shown in Fig. 10. Fig. 11 compares the average of these with absolute predictions of the wall pressure spectrum provided by the Corcos [17] and Chase [18] models, as reported by Howe [19]. The models require values of the boundary layer thickness, skin friction coefficient, edge velocity and convection velocity as input and these were provided from interpolation formulae based on measured values for the wall jet. The convection velocity was set to 41 percent of the edge velocity in accordance with the earlier discussion, and thus agreement in the frequency of the convective ridge is guaranteed. Figs. 12 and 13 show the results of the same analysis for the 40 ms^{-1} data, with the exception that the convection velocity was set to 44 percent of the edge velocity in this case.

At 60 ms^{-1} the basic form of the wavenumber frequency spectrum, revealed in Fig. 10, is consistent with the idealized picture of Fig. 6. The convective ridge, which occurs at around 7 kHz on the horizontal axis, forms an arc that curves towards lower frequencies as the wavenumber angle is increased. The measurements clearly reveal the behavior of the spectrum at frequencies above the convective ridge, where it is seen to decay quite rapidly. The spectra are much more limited at low frequency because the original data here are obscured by background noise levels in the facility (see Fig. 5).

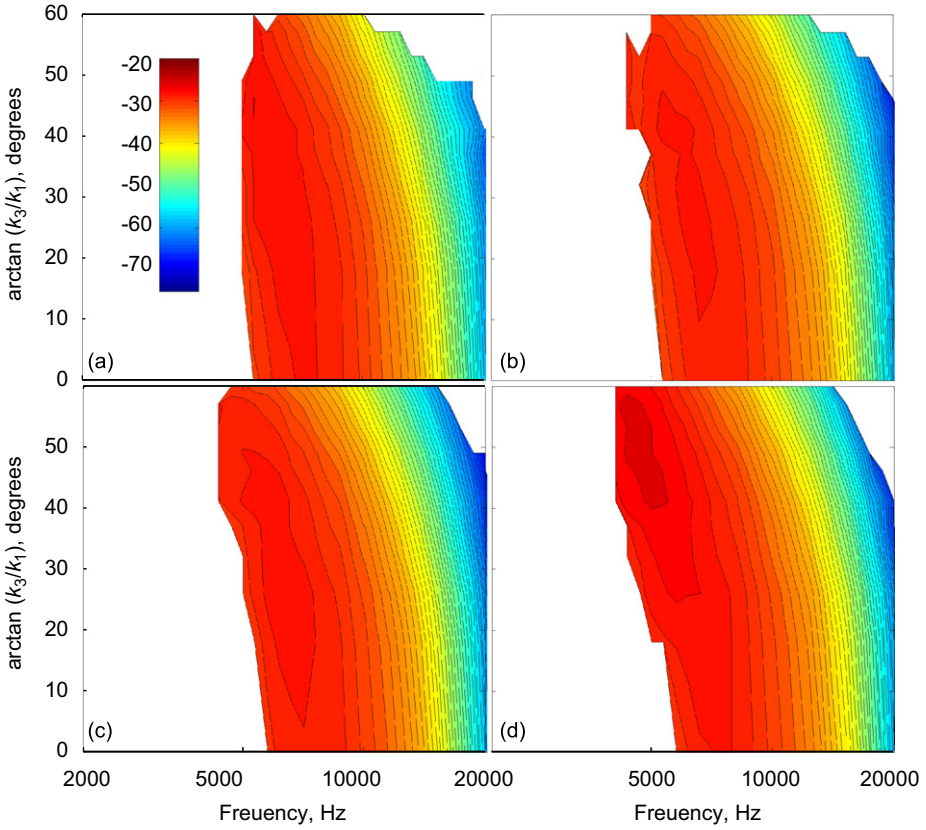

Fig. 10. Absolute wavenumber frequency spectra in dB re 20 μPa (per angular frequency, per wavenumber squared) at 60 ms^{-1} inferred from measurements at receiver angles of (a) $\phi = -1.2^\circ$, (b) $\phi = 20.1^\circ$, (c) $\phi = 40.5^\circ$ and (d) $\phi = 62.6^\circ$.

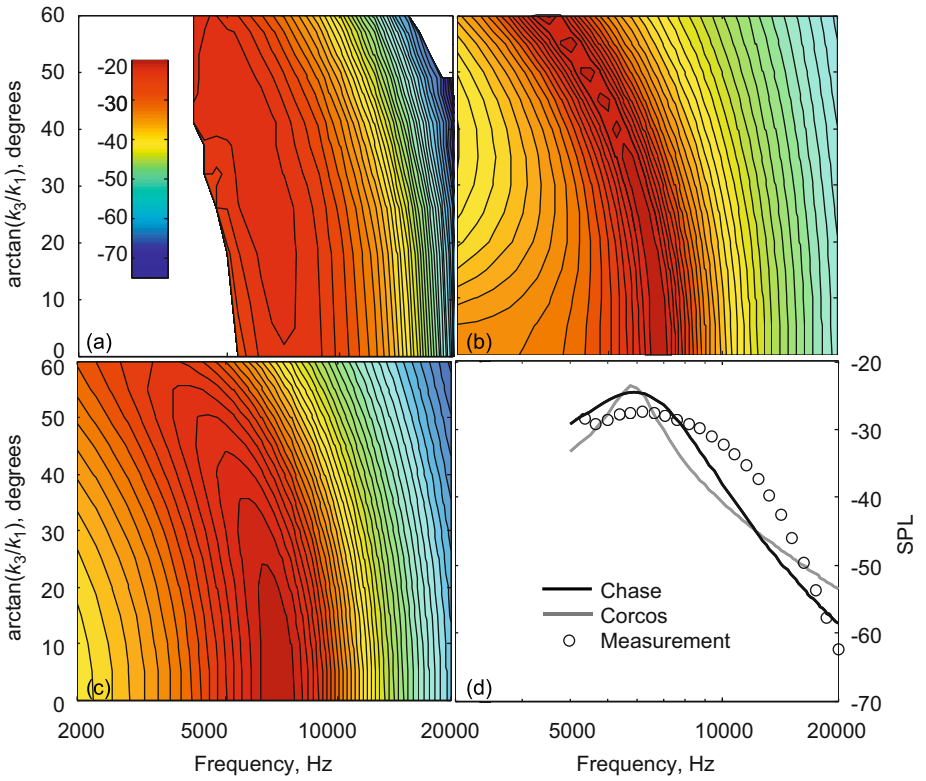

Fig. 11. Absolute comparison of (a) average measured wavenumber frequency spectrum for the 60 ms^{-1} case with (b) the Corcos model and (c) the Chase model. (d) Comparison of measured and model spectra at a wavenumber angle of 32°.

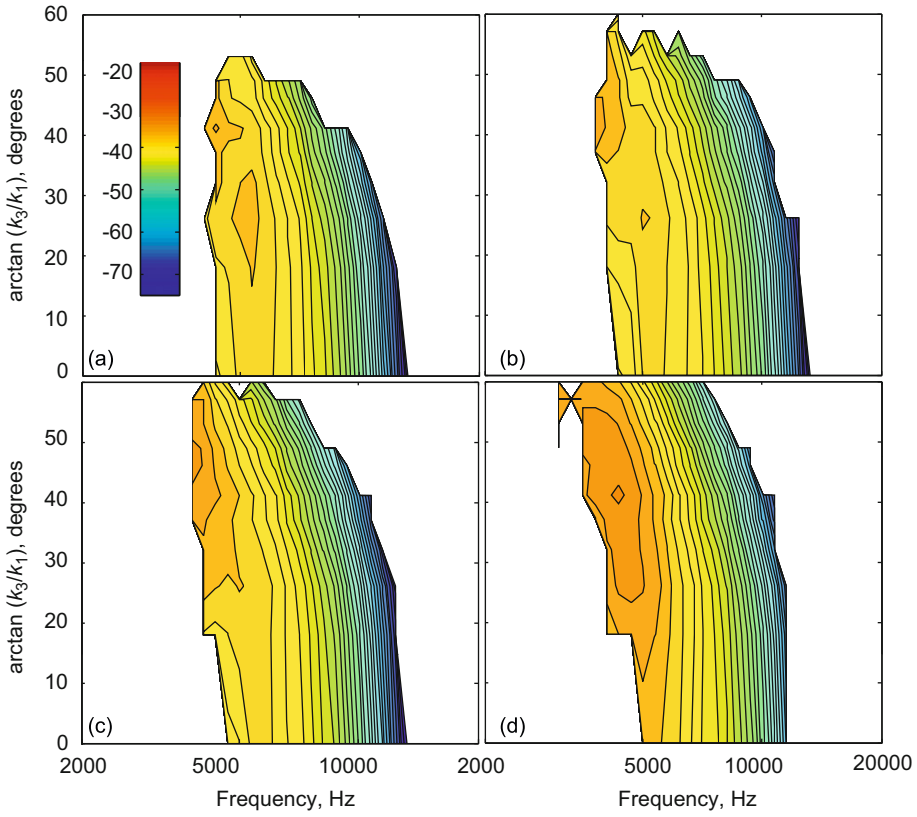

Fig. 12. Absolute wavenumber frequency spectra in dB re 20 μPa (per angular frequency, per wavenumber squared) at 40 ms^{-1} inferred from measurements at receiver angles of (a) $\phi = -1.2^{o}$, (b) $\phi = 20.1^{\circ}$, (c) $\phi = 40.5^{\circ}$ and (d) $\phi = 62.6^{\circ}$.

The same background noise levels (and thus reduced signal to noise ratio) are responsible for some uncertainty in the spectral values on the convective ridge, and this uncertainty may explain the relatively small differences between the spectra measured with the different microphones here. Otherwise, the four estimates of the spectra are remarkably similar. This indicates a close consistency between the measurements and the form of Eq. (6). More specifically, the directivity of the measurements agrees in detail with that predicted by the roughness noise theory [4].

The average of these spectra (or for that matter, any of them individually) makes an interesting comparison with predictions made using the Corcos and Chase models, as shown in Fig. 11. Overall, there is good qualitative agreement, especially between the measurements and the Chase model. Both models, like the measurements, show the convective ridge curving away to lower frequencies as the wavenumber angle is increased. Quantitatively, there are some significant differences between the spectra, seen most clearly in Fig. 11(d) which compares the form of the spectra at a wavenumber angle of 32°. (The comparison at 32° has been chosen as typical of other angles.) The peak spectral value measured at the convective ridge is 3–4 dB lower than that predicted by both models. Furthermore, the high frequency roll off is at first more gradual and then more rapid than that predicted by the models giving the measured spectrum a humpbacked appearance. At the highest frequencies the measured roll off reaches some 40 dB per octave.

The results at 40 ms^{-1} are generally similar to those at 60 ms^{-1} with the exception that the spectral estimates suffer from greater uncertainty (due to the lower signal to noise ratio) particularly around the convective ridge. Accounting for this, however, the wavenumber spectra obtained from the different microphones are still almost identical (Fig. 12), providing further support to the roughness noise theory from which Eqs. (6) and (7) are derived. As before, there is good qualitative agreement between the average wavenumber spectrum and the Corcos and Chase models (Fig. 13). Quantitatively, the measured peak spectral level at the convective ridge is about 8 dB below the values given by the models. One can see again that the models do not accurately capture the more gradual and then more rapid roll off the spectrum at higher frequencies, which again reaches close to 40 dB per octave.

It is important to consider whether the differences with the models could be due to assumptions implicit in the application of Eq. (6). One such assumption is that the ribbed surface (diameter 305 mm) can be treated as infinitely extending. The effect of the finite size of the fetch is, of course, to limit the wavenumber resolution of the measurement, in this case to about 20 rads m^{-1}. At the above convection speeds this implies frequency resolutions of about 20 Hz at 40 m s^{-1} and 30 Hz at 60 m s^{-1}, which are apparently insignificant when compared to the frequency range of the

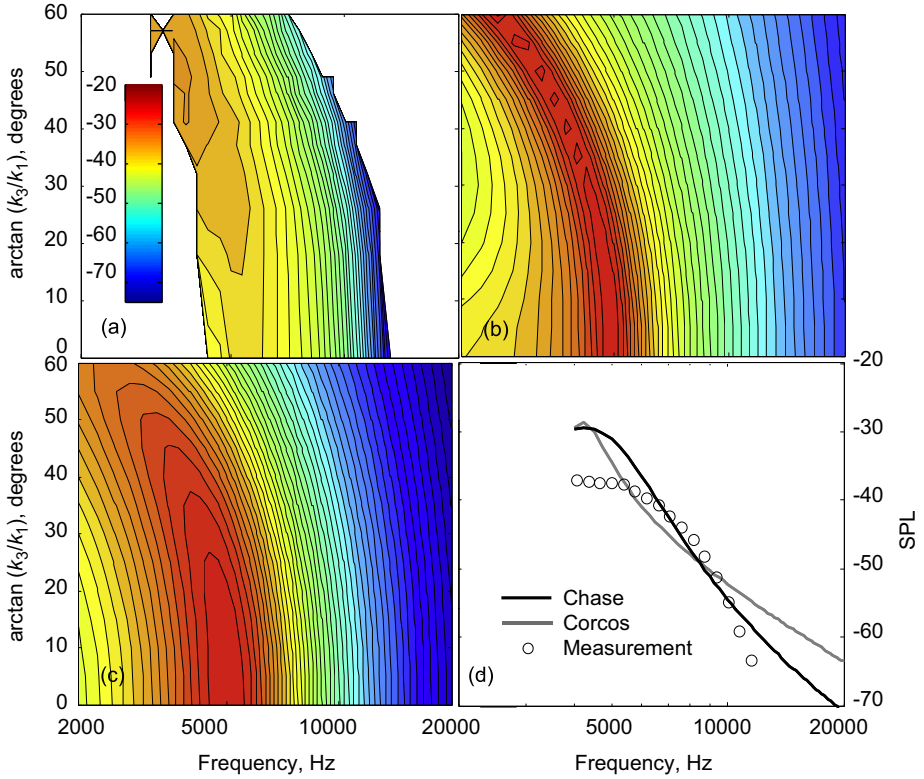

Fig. 13. Absolute comparison of (a) average measured wavenumber frequency spectrum for the 40 ms^{-1} case with (b) the Corcos model and (c) the Chase model. (d) Comparison of measured and model spectra at a wavenumber angle of 32°.

measurements (Figs. 11 and 13). A second approximation is that of a farfield observer. The measurements were made with the microphones close enough to the ribbed surface for there to be a significant variation in observer angle and distance for sound radiated from different portions of the fetch. In effect, therefore, the radiation term $\mathbf{k_w \cdot x}/|\mathbf{x}|^2$ should be replaced by an integral of the distances and angles over the area of the fetch. However, performing this integral exactly yields an answer within 6 percent of the value obtained if the sound source is assumed to be concentrated at the center of the fetch and thus this effect should not be significant either. A third, more important, approximation is that of a sinusoidal surface. In truth, the elliptical surface ridges have higher spatial harmonics, the strongest of which is the first with an amplitude 9.4 dB below the fundamental we have used to characterize the ribbed surface. This harmonic will scatter convective ridge pressure fluctuations with a peak frequency of about twice that produced by the fundamental alone. Because of the higher wavenumber and frequency we would expect these pressure fluctuations to be weaker. Even ignoring this, contamination from the first harmonic would not affect the measured spectra below about 12 kHz for 60 m s^{-1} and 8 kHz for 40 m s^{-1}. This does bring into question the observed high frequency roll-off rates but it is important to note that contributions from the harmonics would only reduce those rates, not increase them. In summary, its seems that the shapes of the measured spectra in the vicinity of the convective ridge are accurate and that differences may be due to inaccuracies in the models. Furthermore, it is clear that the models underestimate the rate of roll off of the actual spectrum at high frequencies.

5. Conclusions

The sound generated by a wall-jet boundary layer flow over a ribbed surface has been measured as a function of observer angle and the angle of the ribs. The ribs had a surface amplitude equivalent to 5 or 7 wall units at the conditions tested and thus were nearly hydrodynamically smooth. Applying the theory of roughness noise to such a situation gives a precise and simple relationship between the measured sound and the wavenumber frequency spectrum of the wall pressure. Overall the sound measurements confirm in detail the applicability of this relationship and the roughness noise theory from which it is derived, particularly the theoretical predictions of directivity. They also clearly demonstrate the measurement of the wall pressure wavenumber frequency spectrum using far field sound at a wavenumber set by the spacing of the ribs. As such, it is possible to measure the wall pressure wavenumber frequency spectrum on scales far smaller than that which could be measured using conventional surface pressure transducers. The measured wall pressure wavenumber frequency spectra bear a close similarity to Corcos' [17] and Chase's [18] model forms. There are differences,

however, in peak spectral levels on the convective ridge and in the high frequency decay that occurs at higher rates than assumed in the models.

Acknowledgments

The authors would like to thank the Office of Naval Research, in particular Dr. Ki-Han Kim, for their support under grant N00014-08-1-0934. We would also like to express our thanks to Mr. Matthew Rasnick for his work in making the mean velocity and turbulence measurements.

References

[1] B. Arguillat, Measurements of the wavenumber-frequency spectrum of wall pressure fluctuations under turbulent flows, *11th AIAA/CAS Aeroacoustics Conference*, Monterey CA, May 2005, AIAA Paper 2005–2855.
[2] S. Glegg, W. Devenport, The far field sound from rough wall boundary layers, *Proceedings of the Royal Society of London Series* 465 (2009) 1717–1734.
[3] C.H. Sherman, H.K. Sung, B.H. Buehler, Measurement of the turbulent boundary layer wave-vector spectrum, *Journal of the Acoustical Society of America* 88 (1990) 386–390.
[4] T.M. Farabee, F.E. Geib, Measurement of boundary layer pressure fluctuations at low wavenumbers on smooth and rough walls, NCA-vol. 11, Flow Noise Modeling Measurement and Control, *American Society of Mechanical Engineers*, 1991, pp. 55–58.
[5] W.K. Blake, *Mechanics of Flow Induced Sound and Vibration*, Academic Press, Orlando, 1986.
[6] D. Grissom, B. Smith, W. Devenport, S. Glegg, Rough wall boundary layer noise: an experimental investigation, *13th AIAA/CEAS Aeroacoustics Conference*, Rome, Italy, May 2007, AIAA-Paper 2007–3418.
[7] B. Smith, W. Alexander, W. Devenport, S. Glegg, D. Grissom, The relationship between roughness noise and the near-field pressure spectrum, *14th AIAA/CEAS Aeroacoustics Conference*, Vancouver BC, May 2008, AIAA Paper 2008–2904.
[8] J. Anderson, D. Stewart, M. Goody, P. Zoccola, Sound from flow over a rough surface, *ASME Mechanical Engineering Congress and Exposition*, November 2007, Seattle WA, IMECE2007-41847.
[9] Y. Lui, A.P. Dowling, H.-C. Shin, Measurement and simulation of surface roughness noise using phased microphone arrays, *Journal of Sound and Vibration* 314 (2008) 95–112.
[10] D. Grissom, A study of sound generated by a turbulent wall jet flow over rough surfaces, PhD Dissertation, Virginia Tech, 2007. Avail: ⟨http://scholar.lib.vt.edu/theses/available/etd-07192007-123339/⟩.
[11] B. Smith, Wall jet boundary layer flows over smooth and rough surfaces, PhD Dissertation, Virginia Tech, 2008. Avail: ⟨http://scholar.lib.vt.edu/theses/available/etd-05082008-144350/⟩.
[12] R. Narasimha, K.Y. Narayan, S.P. Parthasarathy, Parametric analysis of turbulent wall jets in still air, *Aeronautical Journal* 77 (1973) 355–359.
[13] I. Wygnanski, Y. Katz, E. Horev, On the applicability of various scaling laws to the turbulent wall jet, *Journal of Fluid Mechanics* 234 (1992) 669–690.
[14] P. Bradshaw, M. Gee, Turbulent wall jets with and without an external stream, Aeronautical Research Council Reports and Memoranda, R. & M. No. 3252, 1962.
[15] C.K.W. Tam, K.B.M.Q. Zaman, Subsonic jet noise from nonaxisymmetric and tabbed nozzles, *AIAA Journal* 39 (2000) 592–599.
[16] W.K. Blake, Turbulent boundary-layer wall-pressure fluctuations on smooth and rough walls, *Journal of Fluid Mechanics* 44 (1970) 637–660.
[17] G.M. Corcos, The structure of the turbulent pressure field in boundary layer flows, *Journal of Fluid Mechanics* 18 (1964) 353–378.
[18] D.M. Chase, The character of the turbulent wall pressure spectrum at subconvective wavenumbers and a suggested comprehensive model, *Journal of Sound and Vibration* 112 (1987) 125–147.
[19] M.S. Howe, *Acoustics of Fluid Structure Interactions*, Cambridge University Press, Cambridge, UK, 1998.